Atmospheric Environment 86 (2014) 228–240

Contents lists available at ScienceDirect

Atmospheric Environment

journal homepage: www.elsevier.com/locate/atmosenv

In-situ measurements of atmospheric aerosols by using Integrating Nephelometer over a semi-arid station, southern India

K. Rama Gopal [a,*], S.Md. Arafath [a], A.P. Lingaswamy [a], G. Balakrishnaiah [a], S. Pavan Kumari [a], K. Uma Devi [a], N. Siva Kumar Reddy [a], K. Raja Obul Reddy [a], M. Penchal Reddy [a], R.R. Reddy [a], S. Suresh Babu [b]

[a] Aerosol & Atmospheric Research Laboratory, Department of Physics, Sri Krishnadevaraya University, Anantapur 515 003, Andhra Pradesh, India
[b] Space Physics Laboratory, Vikram Sarabhai Space Centre, Trivandrum 695 022, Kerala, India

HIGHLIGHTS

- The σ_{sp}^{550} is found to be 7.8%, reduction from weekdays to weekends.
- The low backscattering ratio is observed during the post-monsoon and higher in the summer.
- The boundary layer height is negatively correlated ($R = -0.68$) with σ_{sp}^{550}.
- A significant +ve correlation has been observed between σ_{sp}^{550} and BC.
- RH versus σ_{sp}^{550} for ambient aerosols shows positive relation where as WS and AT is showed reciprocally.

ARTICLE INFO

Article history:
Received 28 September 2013
Received in revised form
5 December 2013
Accepted 8 December 2013
Available online 27 December 2013

Keywords:
Nephelometer
Scattering coefficient
Backscattering coefficient
Scattering Ångstrom exponent
Backscattering ratio and asymmetry parameter

ABSTRACT

Continuous real-time measurements of aerosol scattering properties were investigated at Anantapur (14° 62′ N, 77° 65′ E, 331 m asl), a semi-arid region in southern India for the period of January 2011–December 2011, using a three-wavelength Integrating Nephelometer. Aerosols scattering properties like the scattering coefficient (σ_{sp}), backscattering coefficient (σ_{bsp}), scattering Ångstrom exponent (Å), backscattering ratio (b_λ) and asymmetry parameter (g_λ) were measured for the period of study. The average values of (±standard deviation) σ_{sp}, σ_{bsp} at 550 nm (σ_{sp}^{550}, σ_{bsp}^{550}) and $Å_{(700/450)}$ were found to be 97 (±9.2) M m^{-1} and 14 (±0.93) M m^{-1} and 1.02 (±0.3), respectively. The estimated average values of b_λ and g_λ at 550 nm from σ_{sp}^{550} and σ_{bsp}^{550} were 0.13 (±0.09) and 0.59 (±0.1), respectively. The maximum asymmetry parameter at 550 nm was found to be 0.63 ± 0.01 in the month of October and minimum (0.52 ± 0.03) during March, which shows the opposite trend with backscattering ratio. Significant correlation coefficients were noticed between different aerosol optical properties. The highest values of σ_{sp}^{550} were observed during weekdays whereas low values during weekends. Scattering Ångstrom exponent for the summer and winter seasons has been consistent with the input of fine mode particles from anthropogenic origin.

1. Introduction

Atmospheric aerosol particles are one of the most variable components of the Earth's atmosphere and are known to influence the energy budget and climate. Aerosol particles affect the Earth's radiative balance and climate directly by absorbing and scattering of solar radiation (Haywood and Shine, 1997; Foster et al., 2007) and indirectly supports for cloud condensation and thus changing the microphysical properties of clouds (Kaufman et al., 2005; Foster et al., 2007). The magnitude and sign of the aerosol forcing effect are determined, in part or by both the horizontal and vertical distribution of the aerosol particles (Haywood and Ramaswamy, 1998). Also, aerosol particles play a major role in atmosphere chemistry and so affect the densities of other minor atmospheric constituents like ozone (Schwartz et al., 1995). Furthermore, aerosol particles have been implicated in human health effects (Dockery and Pope, 1996) and visibility reduction in urban and regional areas (Horvath, 1995). Knowledge of the light scattering properties of atmospheric aerosol particles is of vital importance in estimating the radiative forcing of climate and in

* Corresponding author.
E-mail address: krgverma@yahoo.com (K. Rama Gopal).

1352-2310/$ – see front matter © 2013 Elsevier Ltd. All rights reserved.
http://dx.doi.org/10.1016/j.atmosenv.2013.12.009

global radiation budget studies. Uncertainties in the global aerosol direct and indirect effects are nearly the same or twice as much as the magnitude of the effect itself as estimated by the International Panel on Climate Change (IPCC) in its 4th assessment report (IPCC, 2007). The optical properties of aerosols are related to both their chemical composition and particle size distributions. The atmospheric aerosols in different regions consist of varying composition and size mode, which lead to different radiative impacts on regional climate.

The backscattering ratio, is the ratio of light scattered in the backward hemisphere to the total light scattered by a particle or group of particles. The backscattering ratio has also been used to infer the particle properties *in situ*. The backscattering ratio is found to be used to derive the slope of the particle size distribution and also provides an estimate of the bulk refractive index of particles in the atmosphere. Asymmetric parameter (g) is another parameter which also depends both on the size distribution and composition of aerosol particles and also a function of the relative humidity. Radiative transfer computations use parameterizations of the angular distributions of scattered light or the aerosol phase functions of different aerosol distributions. Many workers have been dedicated to study the aerosol optical properties and their variation at different locations worldwide (Bodhaine and Dutton, 1993; Bodhaine, 1996; Parameswaran et al., 1998; Bergin et al., 2001; Formenti et al., 2002; Colland Coen et al., 2007; Lyamani et al., 2008; Andreae et al., 2008; Jung et al., 2009; Pereira et al., 2011).

In this paper, we report the intensive measurements of aerosol optical properties such as aerosol scattering and Backscattering coefficients over a semi-arid region in southern India, and then analyzed their diurnal variation. Secondly, correlation between aerosol optical parameters was investigated by scattered plots. The influence of meteorological parameters on the aerosol scattering properties has also been analyzed. This study helps in understanding the aerosol scattering effects in the context of regional and global climate change.

2. Site description

Anantapur district in Rayalaseema region (14°62′ N, 77°65′ E) of Andhra Pradesh is geographically situated in a semi-arid zone and occupies the second place to Rajasthan. Anantapur district is the driest part of the state of Andhra Pradesh. Nearly 85 percent of the population is affected by drought in this district, due to low rainfall, high temperature and severe dry winds during monsoon periods. The observation site, Sri Krishnadevaraya University (SKU: 14°62′ N, 77°65′ E and 331 m above sea level) is situated at about 12 km away from the southern edge of the Anantapur town (Fig. 1). The study area is also at a relatively short distance from two national highways (NH 7 and NH 205) and the town area is situated between north and southwest side of the sampling site (Balakrishnaiah et al., 2011a). Within a 50 km radius, this region is surrounded by a number of cement plants, limekilns, brick slab polishing industries and stone crushing machines. Gold mines are situated in southwest region about 40 km away from the observational site. These industries release large quantities of particulate matter into the atmosphere every day. Being far away from east and west coasts, this district is deprived of the full benefits of both the monsoons and consequently droughts are frequently experienced here. It receives the lowest average rainfall of about 450 mm compared to the Andhra Pradesh state average of about 900 mm. During April, June and November months the mean rainfall varies from 10 mm to 50 mm. Clear sky days and full sunshine prevails in the remaining months in this region. Anantapur town and its surroundings experience strong winds (>5 m s^{-1}) during July, August and September months. During October, wind patterns start shifting in direction from southwest to northeast. Most of the winds are prevailing from south-westerly direction during the total observation period. The continental conditions prevailing at this site are responsible for large seasonal temperature differences. On other hand, forest fires and transported dust are the other factors responsible for additional source of aerosol particulates (Badarinath et al., 2009, 2010). During winter, domestic heating (mainly wood, charcoal and diesel central heating) contributes more pollutants to the atmosphere (Kumar et al., 2011).

3. Instrumentation

The Integrating Nephelometer TSI model 3563 has been used to measure the total scattering (7°–170° angular integration) and the hemispheric backscattering (90°–170^{0}) coefficients at three visible wavelengths (450, 550 and 700 nm each with a bandwidth of 50 nm). The instrument is kept on the top floor of a three stored building (12 m). An inverted funnel with screws fitted at the entrance of the instrument to avoid the dust, rain water and insects entering into the system. This instrument draws the ambient air through a stainless steel tubing (Diameter = 3.2 cm and Length = 1.8 m) inlet at a flow rate of 20 LPM, and the sample is illuminated with a halogen lamp and measures scattered light at 450, 550 and 700 nm using three photomultiplier tubes. The nephelometer contains one humidity and two temperature sensors. The humidity sensor and one temperature sensor are located near the sample outlet and the other temperature sensor is located at the sample inlet.

The scattering coefficient shows a minimum dependence on RH at <50% and sharp increase at >80% RH (Anderson and Ogren, 1998; Xu et al., 2002). Calibration of the nephelometer has been carried out twice per year by using CO_2 as high span gas and filtered dry air as low span gas. These data are recorded with a temporal resolution of 1 min, and the zero signals are measured for every 5 min in a hour. The total scattering and backscattering data are corrected on a systematic basis considering the angular truncation errors (Anderson and Ogren, 1998).

The meteorological parameters like Air Temperature (AT), Relative Humidity (RH), Rain Fall (RF), and Wind Speed (WS) have been measured by using Mini Boundary Layer Mast (MBLM) installed near the measurement location. The daily surface wind flow patterns at Anantapur site have been obtained from NCEP/NCAR reanalysis data (http://www.cdc.noaa.gov).

4. Methodology

The scattering and backscattering coefficients at three different wavelengths are measured by using TSI Model 3563 Integrating Nephelometer. The scattering Ångstrom exponent (Å) represents the wavelength dependence of scattering coefficient and can be related to a mean size of the particle. It was calculated using the 450 and 700 nm channels as follows (Pereira et al., 2011).

$$\mathring{A} = -\frac{\log\left(\sigma_{sp}^{\lambda_1}\right) - \log\left(\sigma_{sp}^{\lambda_2}\right)}{\log(\lambda_1) - \log(\lambda_2)} \quad (1)$$

In the above equation $\sigma_{sp}^{\lambda_1}$ and $\sigma_{sp}^{\lambda_2}$ are the scattering coefficients obtained at the wavelengths of λ_1 (700 nm) and λ_2 (450 nm) respectively.

The backscattering ratio is the ratio of the backscattering coefficient over the scattering coefficient at a given wavelengths (450, 550 and 700 nm).

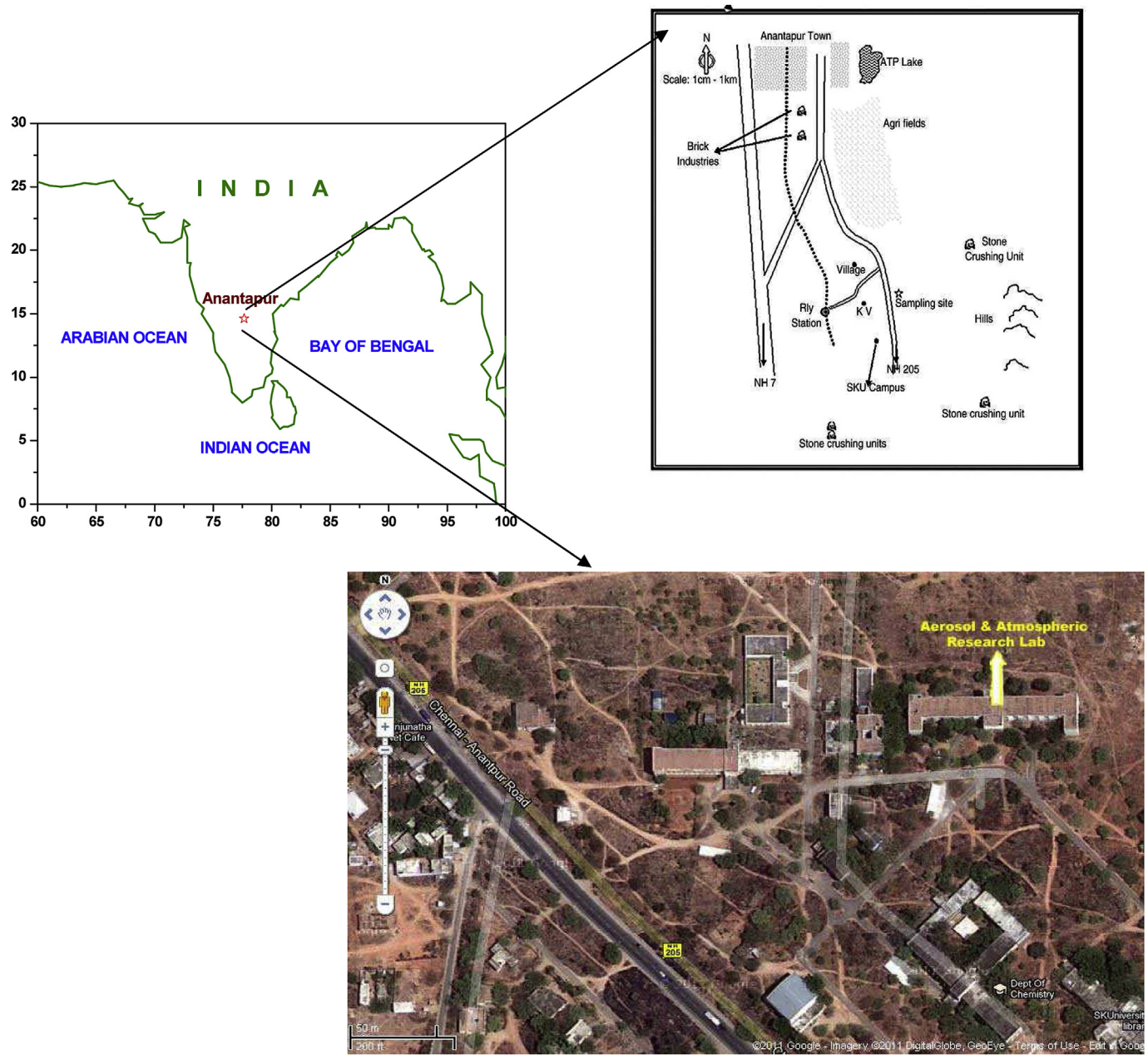

Fig. 1. Geographical location of Anantapur over the India subcontinent and adjoin oceanic regions (top left panel). Also shown road map of the observation site, Sri Krishnadevaraya University (top right panel) and satellite aerial view of monitoring site building in the SKU campus indicated with an arrow head(bottom panel).

$$b_\lambda = \frac{\sigma^\lambda_{bsp}}{\sigma^\lambda_{sp}} \quad (2)$$

Where σ^λ_{sp} and σ^λ_{bsp} are scattering and backscattering coefficients obtained at the same wavelength.

The asymmetry parameter (g_λ) is calculated from the backscattering ratio (b_λ).

$$g_\lambda = -7.143889*b_\lambda^3 + 7.464439*b_\lambda^2 - 3.9356*b_\lambda + 0.9893 \quad (3)$$

Where g_λ and b_λ are asymmetry parameter and backscattering ratio obtained at the same wavelength. The above equation was suggested by Andrews et al. (2006) based on the plot of Wiscombe and Grams (1976) following Henyey–Greenstein approximation for asymmetry parameter.

5. Results and discussion

5.1. Diurnal variation in scattering (σ_{sp}), backscattering (σ_{bsp}) coefficients and scattering Ångstrom exponent (Å)

The measured average diurnal variation of σ_{sp} and σ_{bsp} of atmospheric surface aerosols at three wavelengths (450, 550 and 700 nm) during the study period is shown in Fig. 2. Bi-peak diurnal patterns were observed for σ_{sp} and σ_{bsp} at 0700 LT and 2100 LT, respectively. The diurnal variation of σ_{sp} and σ_{bsp} is mainly

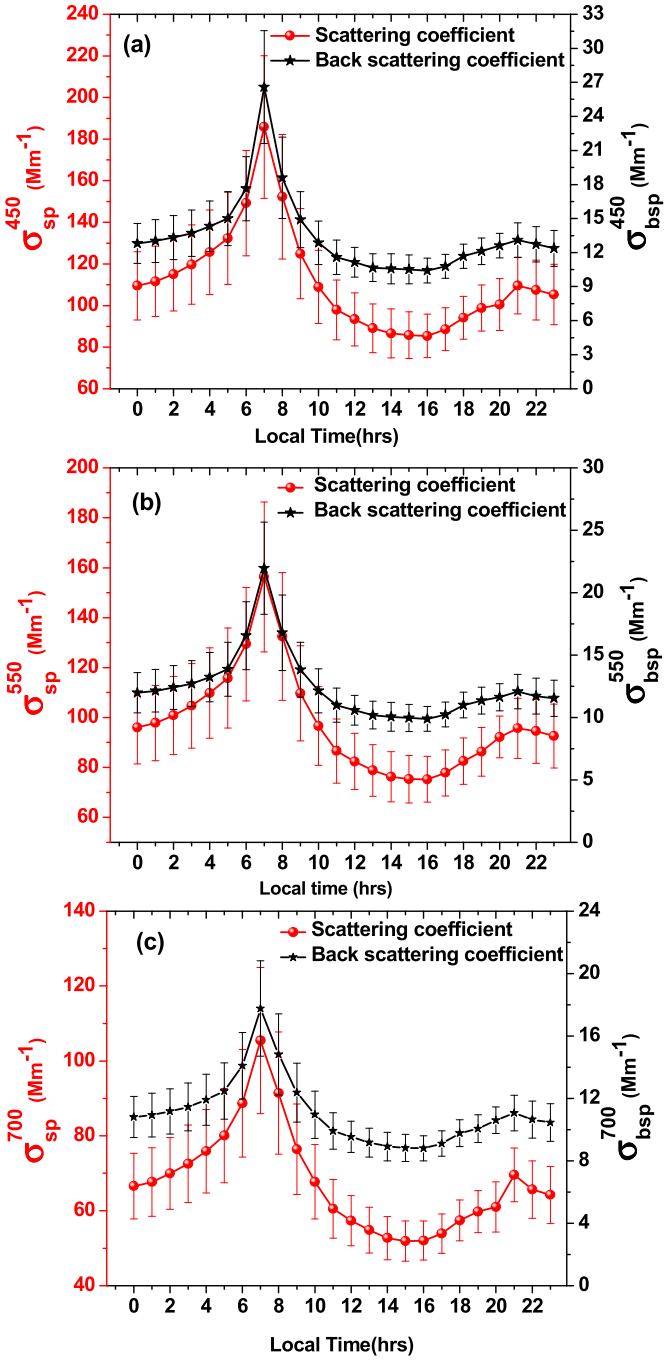

Fig. 2. Diurnal variation (a) scattering and backscattering coefficients at 450 nm,(b) scattering and backscattering coefficients at 550 nm,(c) scattering and backscattering coefficients at 700 nm.

governed by the diurnal cycle of the boundary layer height and local emission pattern as well as wind speed which play a potential role.

The enhancement peak of σ_{sp} and σ_{bsp} was found during the early morning hours that is just after an hour of local sunrise (0700 LT) at different wavelengths are 185.85 ± 34.31 M m^{-1} (450 nm), 156 ± 29.9 M m^{-1} (550 nm), 105.43 ± 19.4 M m^{-1} (700 nm) for σ_{sp} and 26.58 ± 4.9 M m^{-1} (450 nm), 20.76 ± 3 M m^{-1} (550 nm), 16.5 ± 2.7 M m^{-1} (700 nm) for σ_{bsp} respectively. The morning peak is mainly due to the buildup of local anthropogenic activities associated with the traffic rush and the low boundary layer height. During night, the height of the planetary boundary layer (PBL) decreased and the pollutants are entrapped in the lower levels of the atmosphere and leads to high concentrations of aerosols at the surface and results nocturnal peak.

The scattering and backscattering coefficients are declined at the surface during the afternoon hours and obtained minimum values for σ_{sp} and σ_{bsp} are i.e., 85.74 ± 11.2 M m^{-1}(σ_{sp}^{450}), 75.27 ± 9.4 M m^{-1} (σ_{sp}^{550}) and 51.88 ± 5.53 M m^{-1} (σ_{sp}^{700}); 10.51 ± 1.2 M m^{-1}(σ_{bsp}^{450}), 9.96 ± 1.1 M m^{-1} (σ_{bsp}^{550}) and 8.82 ± 0.87 M m^{-1} (σ_{bsp}^{700}) around 1500 LT, respectively. These results are attributed to the boundary layer increase together with the increase in convection throughout the day and also lead the conditions for particle dilution within a larger volume of air.

Fig. 3 highlights the hourly average diurnal variation of the scattering Ångstrom exponent for different wavelength pairs (700/550, 700/450 and 550/450) during the study period. Diurnal variation of Å exhibits similar pattern as that of scattering and backscattering coefficients. Results showed two prominent peaks and one was noticed (primary peak) during the morning hours (1.53 ± 0.03 (550/700), 1.1 ± 0.02 (450/700) and 0.8 ± 0.01 (450/550)) at around 0700 LT and second one (1.46 ± 0.02 (550/700), 1 ± 0.02 (450/700) and 0.7 ± 0.01 (450/550)) at around 2100 LT. This indicates the dominance of fine mode particles over the measurement location. The observed scattering Angstrom exponent during 1100–1600 LT is less which may be due to the dominance of coarse mode particles prevailing in the atmosphere. These particles are mainly transported from the stone crushing industries and the lift of the loose soil through high wind speed prevailing in that region.

5.2. Monthly variation of scattering (σ_{sp}), backscattering (σ_{bsp}) coefficients and scattering Ångstrom exponent (Å)

The monthly evaluations of the daily mean values of scattering and backscattering coefficients at three wavelengths (450, 550 and 700 nm) and scattering Ångstrom exponent for different wavelength pairs (700/550, 700/450 and 550/450) are observed during the study period are shown in Fig. 4(a), (b) and (c). The monthly variations in the above properties are mainly attributed to the prevailing meteorological conditions in respective months. The maximumσ_{sp}^{550}, σ_{bsp}^{550} and $Å_{(700/450)}$ values observed are 140 ± 11.23 M m^{-1}, 18 ± 4.32 M m^{-1} and 1.5 ± 0.09, respectively in the month of January, where as minimum values for σ_{sp}^{550}, σ_{bsp}^{550} and $Å_{(700/450)}$ are noticed as 40 ± 5.23 M m^{-1}, 6 ± 1.32 M m^{-1} and 0.7 ± 0.07 in the month of September. The observed maximum values in the January and February are mainly due to the boundary layer subsidence and leads confinement of aerosols. This type of boundary layer dynamics is due to the surface temperature variation that could be the reason for the maximum scattering coefficient. During this period, the air mass pathway is from northeasterly to the observing site (Fig. 11), which brings mostly the continental air and leads to the enhanced anthropogenic component. Biomass burning, local household biomass burning for cooking, low prevailing temperature and wind speeds (Latha and Badarinath, 2005; Pathak et al., 2010) are responsible for high concentration during this period.

High values of Angstrom exponent were noticed during winter which indicates the dominance of fine mode particles. During summer most of the winds are from westerly, south-westerly (Fig. 11) and bring the moist of the air from adjoining sea regions along with occasional influx of some continental air masses reaching from the North India region. During this episode, forest fires are greatly responsible for the large input of particles detected

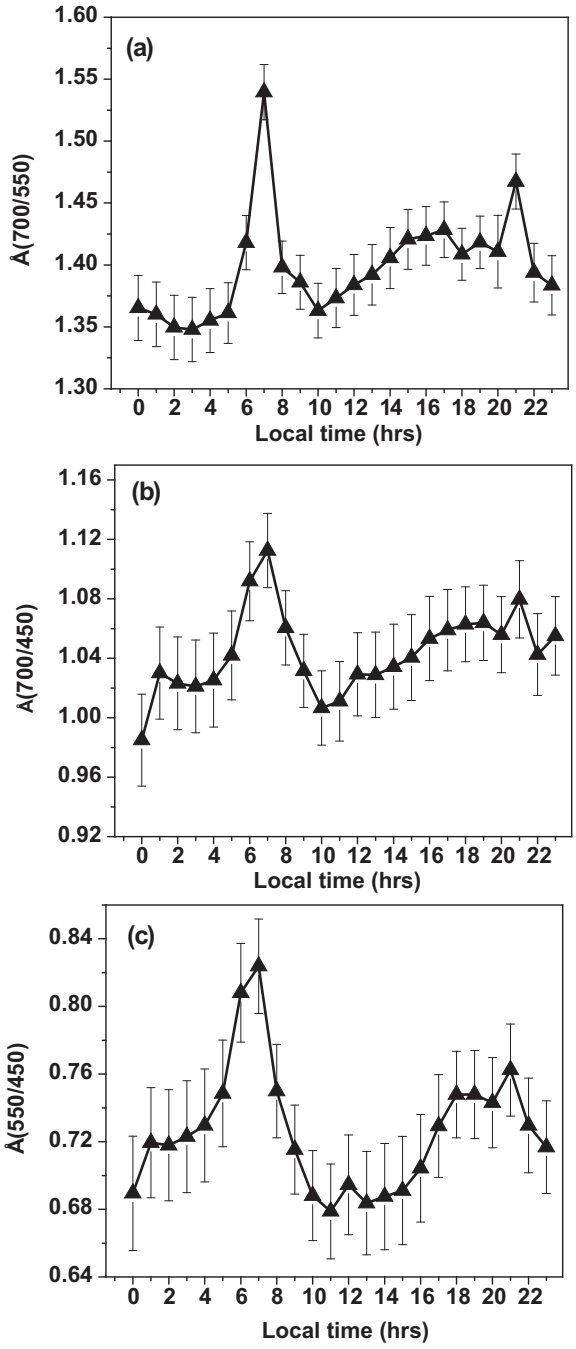

Fig. 3. Diurnal variation (a) scattering Ångstrom exponent at (700/550), (b) scattering Ångstrom exponent at (700/450) and (c) scattering Ångstrom exponent at (550/450).

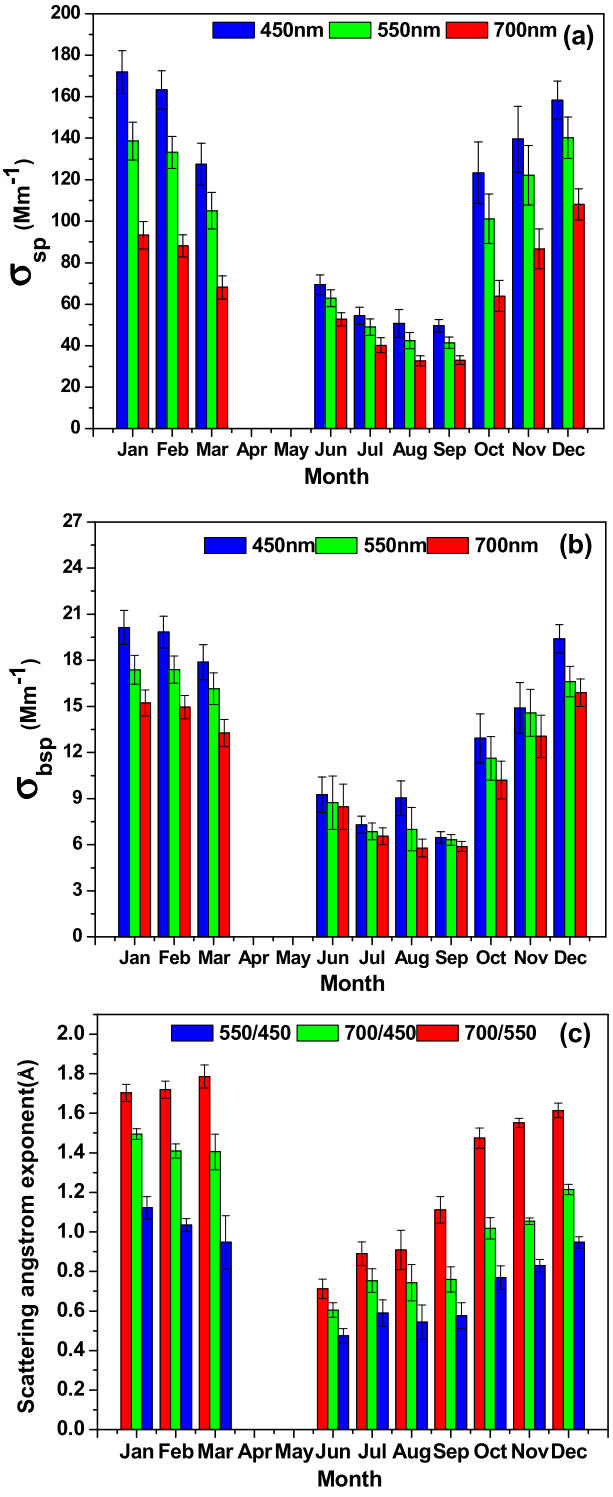

Fig. 4. Monthly mean variation of scattering properties found at Anantapur during the 2011, (a) scattering coefficient (b) backscattering coefficient (c) scattering Ångstrom exponent.

over the site (Balakrishnaiah et al., 2011b). In this period dispersion of aerosols are high owing to the large ventilation coefficient which is a product of mixing height and local wind speed, therefore the surface concentration are relatively low compared to winter months.

Low values of Å were observed during monsoon season which is due to the pollutants carrying winds are mainly from south-westerly and rich with marine air mass. Consequently, in this season coarse particle domination is more. The cloud precipitation scavenging, removal out aerosols are due to overcast and rains, high wind speed, low anthropogenic activities which play a significant role in drastic reduction in the surface concentrations.

5.3. *Weekday and weekend analysis of* σ_{sp}^{550}, σ_{bsp}^{550} *and* $Å_{(700/450)}$

The diurnal hourly average values of scattering properties were measured for weekdays (i.e., Monday–Friday) and weekend days (i.e., Saturday and Sunday), to study the influence of anthropogenic activities like traffic, industries and wood burning etc. over the sampling site and also shown in Fig. 5.

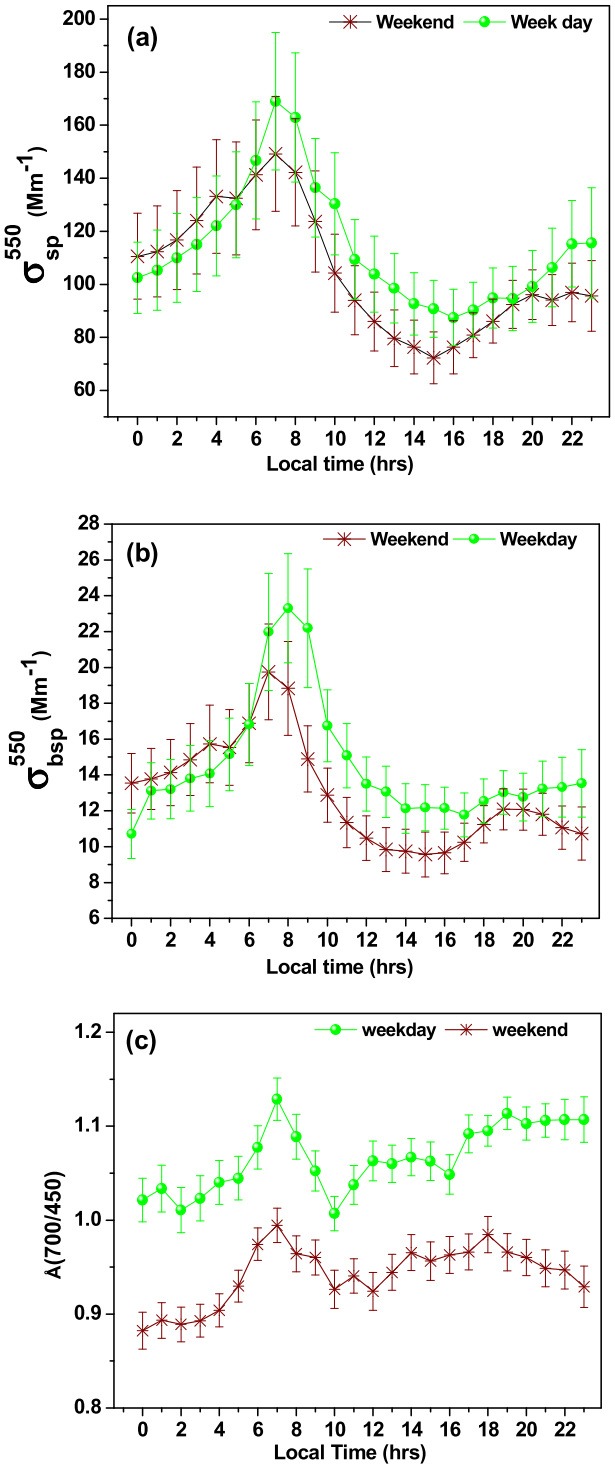

Fig. 5. Temporal variation of measured optical parameters during weekdays and weekends over semiarid region during study period, (a) scattering coefficient at 550 nm (b) backscattering coefficient at 550 nm (c) scattering Ångstrom exponent (700/450).

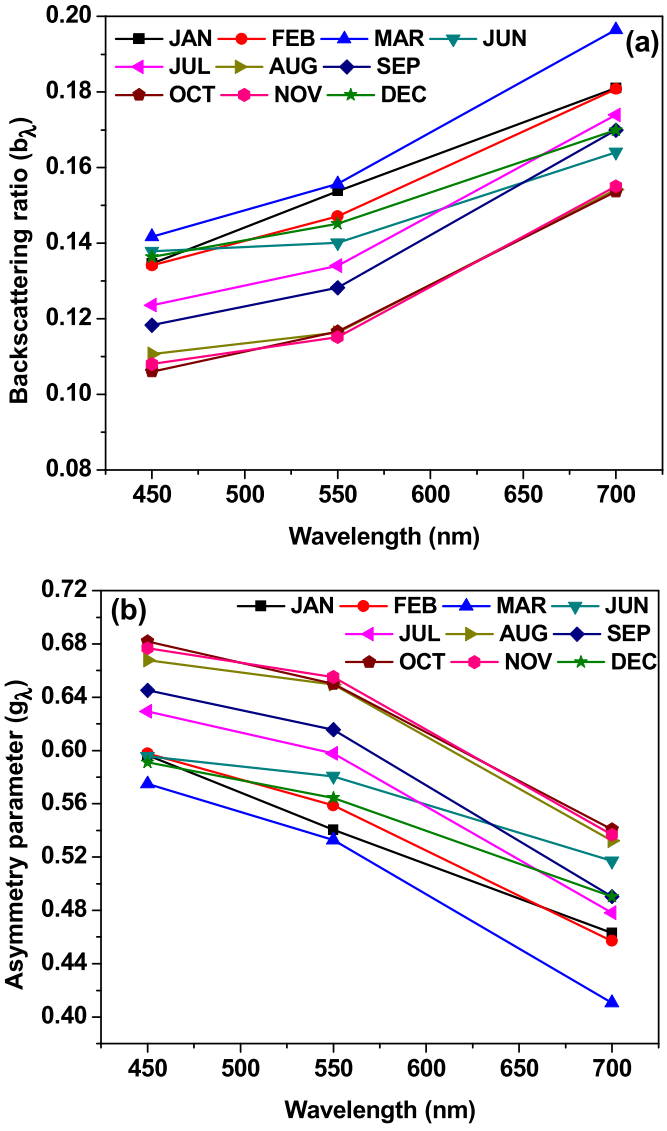

Fig. 6. Spectral variation of (a) backscattering ratio and (b) asymmetry parameter.

The diurnal variation of σ_{sp}^{550},σ_{bsp}^{550} and $Å_{(700/450)}$ for weekdays and weekends shows two predominant note worth peaks in the morning (0700 LT) and in the evening hours (2000 LT). The average diurnal variations of σ_{sp}^{550} were found to be 113 M m^{-1} and 104 M m^{-1} for weekdays and weekends and 7.8% of reduction in the scattering from weekdays to weekends were observed. Similarly 14 M m^{-1} and 11 M m^{-1} have been noticed for σ_{bsp}^{550} during weekdays and weekends respectively and 11% reduction in σ_{bsp}^{550} from weekdays to weekends. The lowest scattering values observed on weekends compared to weekdays are due to the influence of the fine mode aerosols concentration (possibly due to anthropogenic origin). During early morning hours of weekend, the observed higher values are due to capping action of aerosols released from various anthropogenic activities by previous night. As the day progress, there is a continuous increase in the boundary layer height permitting an increased dilution of the aerosol.

Fig. 5(c) presents diurnal variation of the Å exponent during weekdays and weekends which specifies the size distribution of the particles. During the weekdays, $Å_{(700/450)}$ was found to be in the range of 0.9–1.7, whereas during the weekends $Å_{(700/450)}$ was found in the range of 0.4–1.2. The observed $Å_{(700/450)}$ is high which represents fine mode dominance during the weekdays due to enhancement of anthropogenic activities (vehicular sources, burning etc.,) over the study area.

5.4. Spectral variation of backscattering ratio and asymmetry parameter

The Fig. 6(a) shows the spectral variation of average backscattering ratio for different months over the sampling site during the

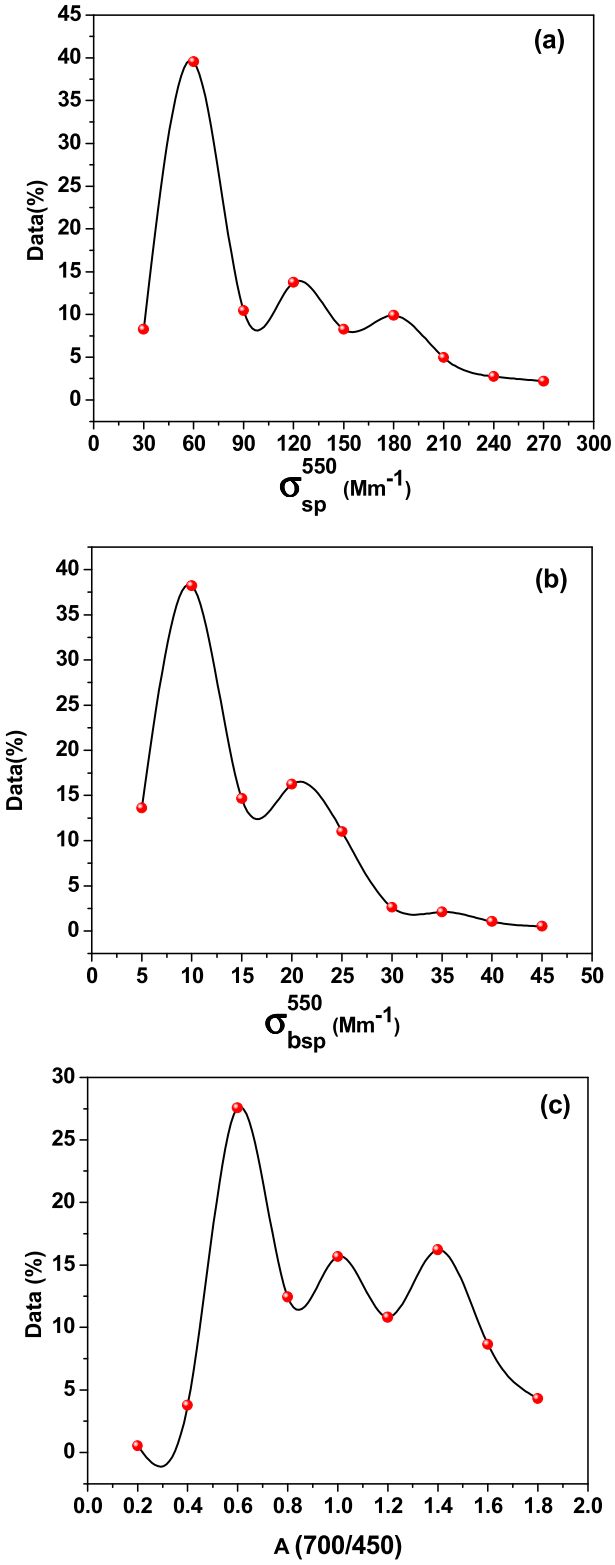

Fig. 7. Relative frequency distributions of (a) scattering coefficient (550 nm), (b) backscattering coefficient (550 nm) (c) Scattering Ångstrom exponent (700/450).

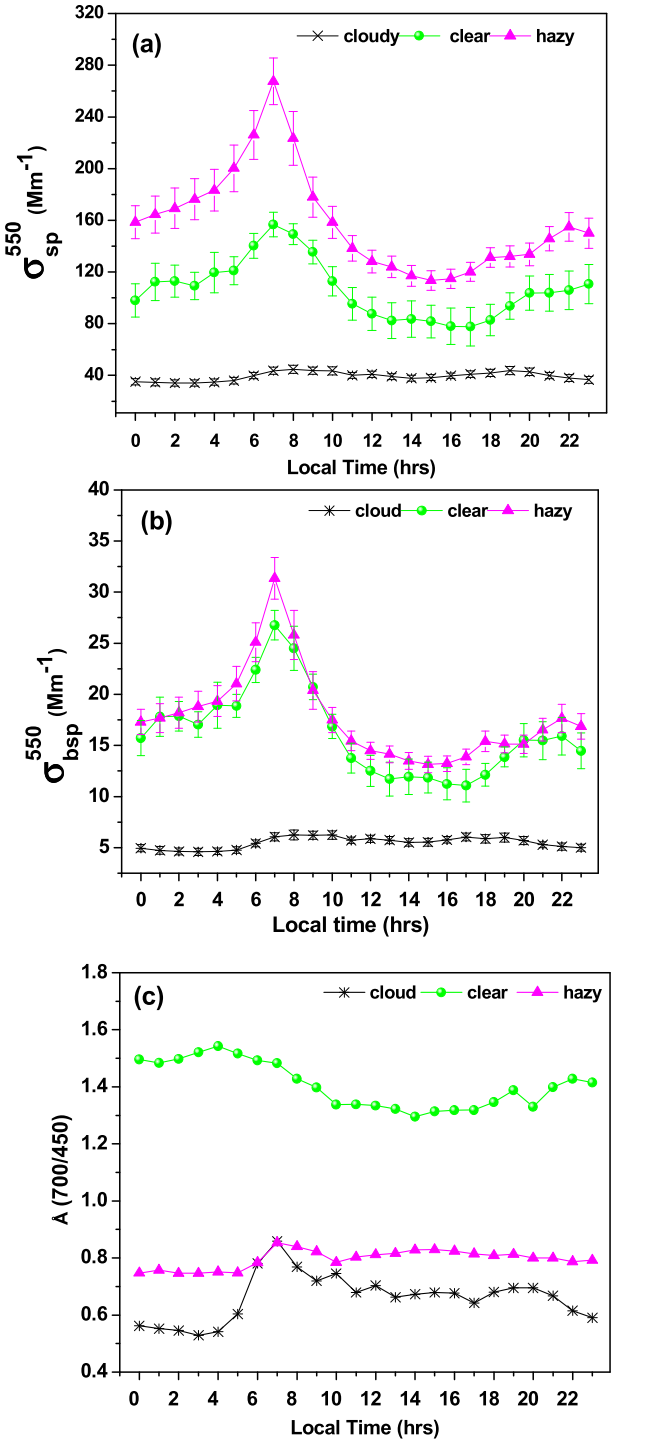

Fig. 8. Measured diurnal cycle of optical parameters during clear, hazy and cloudy episodes (a) scattering coefficient (550 nm) (b) backscattering coefficient (550 nm) (c) scattering Ångstrom exponent (700/450).

study period. The backscattering ratio is very useful characteristic parameter for describing the cooling effect of aerosol on climate, as it is a measure of the fraction of the scattered radiation that is returned to space. Backscattering ratio is weakly dependent on concentration, provides us wealth information on the characteristics of the particulate material, such as the index of refraction and the angular dependence of scattering which are necessary for the estimation of aerosol scattered diffuse radiation reaching the ground. One of the main objectives is to examine the behavior of the spectral particulate backscattering ratio in-situ, both in terms of its absolute magnitude and its variability across three visible wavelengths.

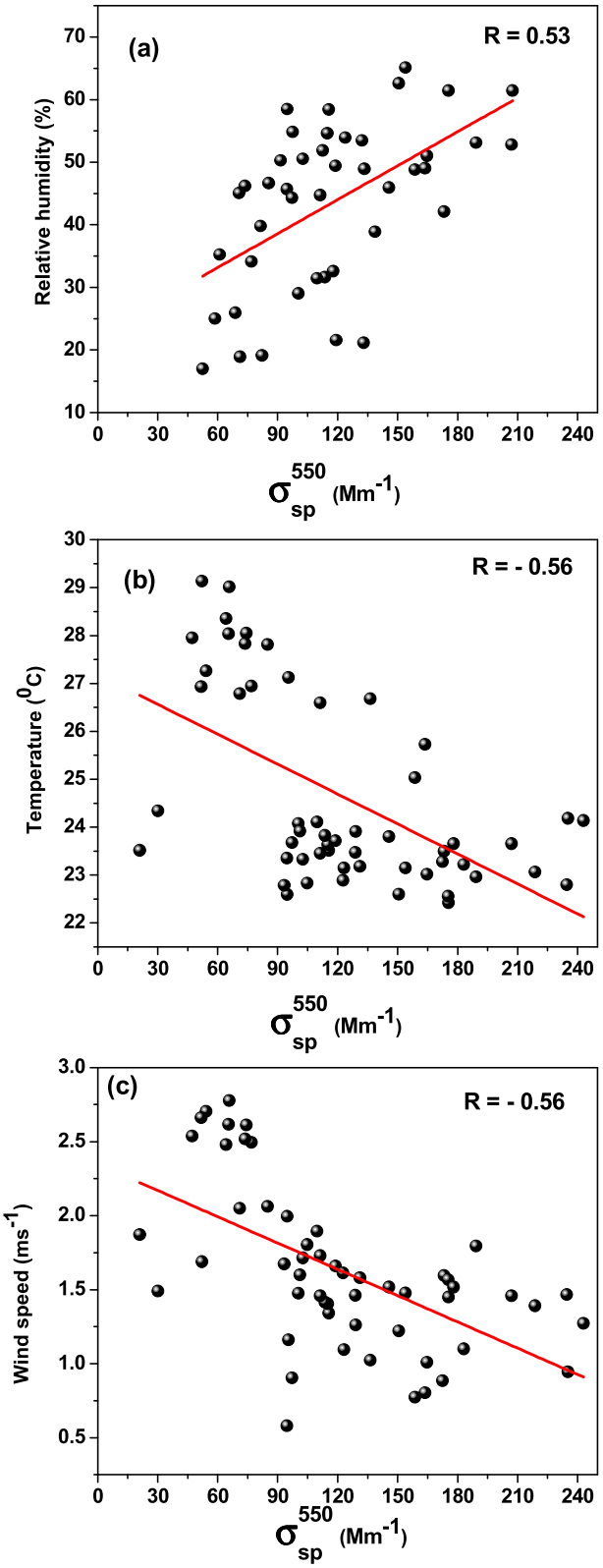

Fig. 9. Scatter plot of the scattering coefficient (550 nm) against metrological parameter (a) relative humidity, (b) air temperature and (c) wind speed during study period.

The backscattering ratio at 550 nm exhibits a little variability during period of study and lies in the range 0.12–0.16. The higher backscattering ratio at 550 nm was observed in the month of March (0.15) and lower in the month of October (0.11). The observed low backscattering ratio during the October shows the dominance of coarse mode particles and found higher in the month of March. Mie theory predicts that backscattering ratio should be higher for fine mode aerosol particles. These results are in good agreement with Formenti et al. (2001) and Andreae et al. (2002). The value of backscattering ratio was 0.13 reported for the Negev desert by Formenti et al. (2001). Andreae et al. (2002) also reported that the mean backscattering ratio was 0.13 over Sde Boker (Israel), under continental pollution conditions.

However several studies have been found that the backscattering ratio values are higher for dust and particles from forest fires than other type of aerosol particles (Carrico et al., 2003; Doherty et al., 2005). In previous studies it was found (based on theory and observations) that the backscattering ratio was sensitive to composition (organic content and particle size distribution) (Twardowski et al., 2001; Boss et al., 2004).

The backscattering ratio and the asymmetry parameter are independent on the amount of aerosol presence in the atmosphere and helps in determining aerosol intensive properties. Instead, this ratio provides information about characteristics of the bulk particle population (e.g. particle composition, mean size, shapes etc.).

The Fig. 6(b) describes the spectral variation of asymmetry parameter (for different month) which exhibits opposite pattern to the backscattering ratio. The asymmetry parameter is a simple, single valued representation of the angular scattering and plays a key role in controlling the aerosol contribution to the forcing (Pandithurai et al., 2008) which depends on the size and composition of the particles. It is possible to derive the asymmetric parameter from backscattering ratio employing the Equation (3) given above. This optical property (asymmetry parameter) is useful in the estimating aerosol forcing of climate and is used in most radiative transfer calculations. The values of asymmetry parameter show the decrease trend as wavelength increases in the visible spectral region. This behavior is in good agreement with the view of Pandithurai et al. (2008). It is pertinent to mention that significant dependence on wavelength is mainly due to the location or air mass type over the measurement site. The mean values derived for asymmetry parameter at 550 nm ranged between 0.50 and 0.70 over the sampling site. The maximum asymmetry parameter at 550 nm was found to be 0.65 in the month of October due to the domination of large particles over the region where as minimum of 0.53 in the month of March, mainly due to small abundance particles loading from the stone crushing activities, air lifting soil particles, and transport.

Ramachandran and Rajesh (2008) reported that asymmetry parameter at 550 nm is corresponding to 30% RH in the 0.3–0.6 range over India. The median values range from 0.57 for free tropospheric aerosol to 0.65 for marine aerosol at 550 nm wavelength (Fiebig and Ogren, 2006). Formenti et al. (2000) found slightly higher values (0.72–0.73) for Saharan dust aerosol. The asymmetry parameter increases while backscattering ratio decreases and the similar type of findings were also reported by Andrews et al. (2006).

5.5. Frequency distribution of σ_{sp}^{550}, σ_{bsp}^{550} and $\mathring{A}_{(700/450)}$

Fig. 7(a), (b) and (c) shows the measured daily average frequency distribution of σ_{sp}^{550}, σ_{bsp}^{550} and $\mathring{A}_{(700/450)}$ for the study period. The scattering Ångstrom exponent values provide the information about the average size distribution of the particles. In the view of the above the percentage occurrence are grouped for the $\mathring{A}$ values into two categories i.e., $\mathring{A}$ <1 (coarse mode aerosols) and $\mathring{A}$ >1 (fine mode aerosols). The significant percentage occurrence of the $\mathring{A}$ values in coarse mode and fine mode category may not purely represent the aerosol size associated with it but is dominated by the

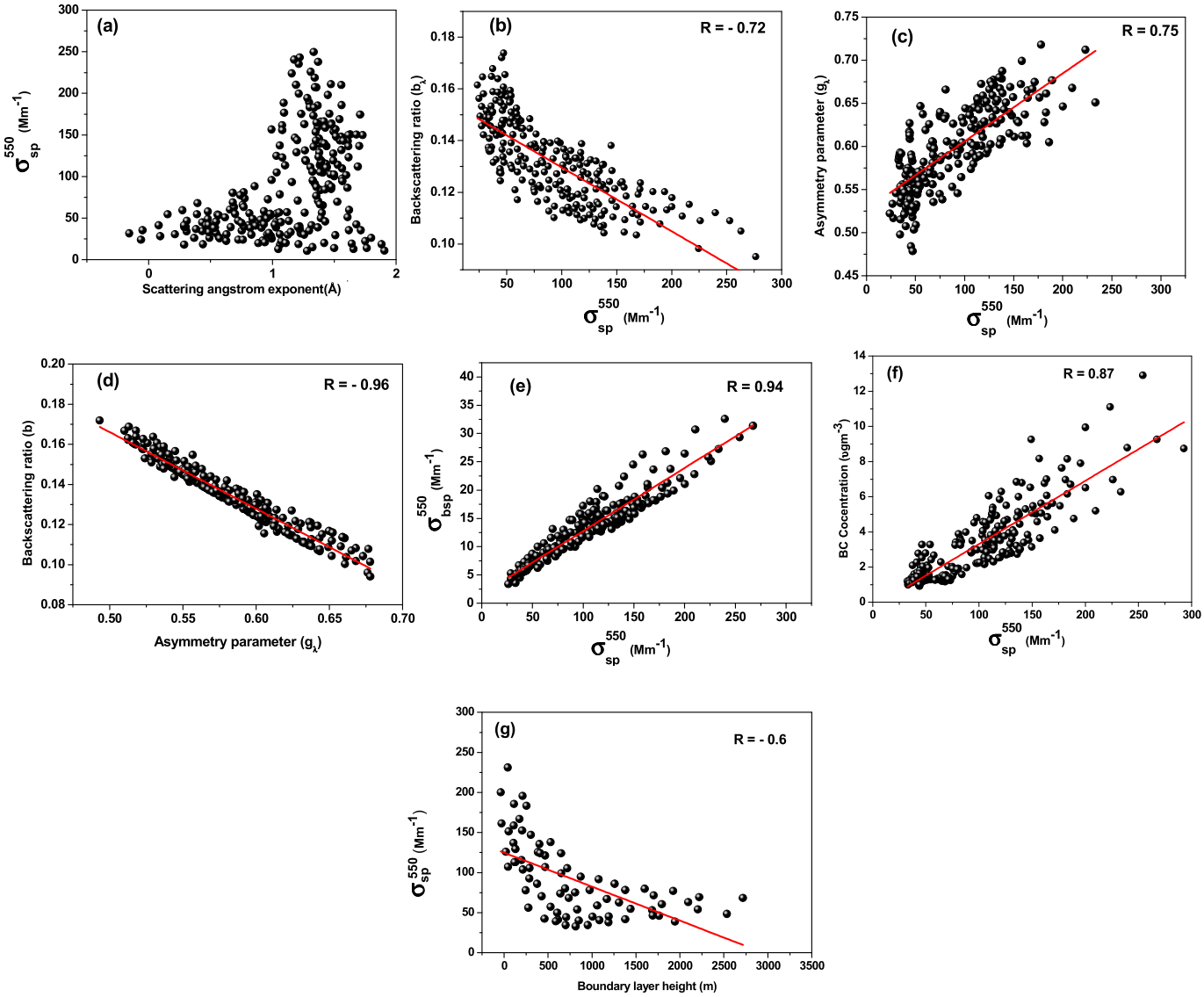

Fig. 10. Systematic variability of scattering coefficient at 550 nm with (a) scattering Ångstrom exponent (b) backscattering ratio (550 nm) (c) asymmetry parameter (550 nm) (d) backscattering ratio (550 nm) vs asymmetry parameter (550 nm) (e) scattering coefficient (550 nm) vs backscattering coefficient (550 nm) (f) scattering coefficient (550 nm) vs black carbon aerosols (BC) (g) scattering coefficient (550 nm) vs boundary layer height.

respective size in the said category. It was observed that in the sampling site, 40% of σ_{sp}^{550} data points lie in the range of 30–60 M m^{-1}, 15% of data points lie in the range of 90–120 M m^{-1} and 3% of data points lie in the range of 240–270 M m^{-1}. On other hand 37% of σ_{bsp}^{550} the data points lie in the range of 5–10 M m^{-1}, 15% of σ_{bsp}^{550} values lie in the range of 15–20 M m^{-1}. The least data points (2%) were observed in the range of 40–45 M m^{-1}. The large variations in the $Å_{(700/450)}$ observed during the study period was in between 0.2–1.8, which shows a higher frequency for $Å_{(700/450)}$. It was pertinent to maintain that 29% of all $Å_{(700/450)}$ values lie in the range of 0.4–0.6, 27% lie in the range of 0.6–1.0 and the reaming 44% of $Å_{(700/450)}$ values lie in the range 1.0–1.8. This result highlights the dominance of aerosols in the fine-mode during the study period over the sampling site. The modal value observed around 1.3, indicating the dominance of fine-mode aerosols during the winter and is due to biomass burning and fossil fuel combustion sources. The observed $Å_{(700/450)}$ values are high and found to be around 0.2–1.0. This is mainly due to the anthropogenic activities prevailing around the observational site (Industries, brick factories, stone crushing etc). The anthropogenic activities play a major role in the formation of nucleation and growth of cloud droplets especially while relative humidity is very high.

5.6. Aerosol optical properties during clear, hazy and cloudy conditions

The daily mean relative humidity (RH) is to be taken as RH < 35% for a clear, 40 < RH < 65% for a hazy and RH > 65% for a cloudy conditions in the variations of σ_{sp}^{550}, σ_{bsp}^{550} and $Å_{(700/450)}$. The classification of clear, hazy and cloudy days is based on the meteorological data collected from the Mini Boundary Layer Mast (MBLM) station, which was installed at the observation site. Fig. 8(a) and (b) shows the diurnal cycles of σ_{sp}^{550} and σ_{bsp}^{550} during clear, hazy and cloudy periods. The average σ_{sp}^{550} value is noted as 160 M m^{-1} during the hazy periods and 40 M m^{-1} during the cloudy episodes. Maximum values are found in the hazy episodes and evidenced by the maximum scattering and are due to dust, smoke, and vapor presence in the atmosphere. Low σ_{sp}^{550} and σ_{bsp}^{550} values measured

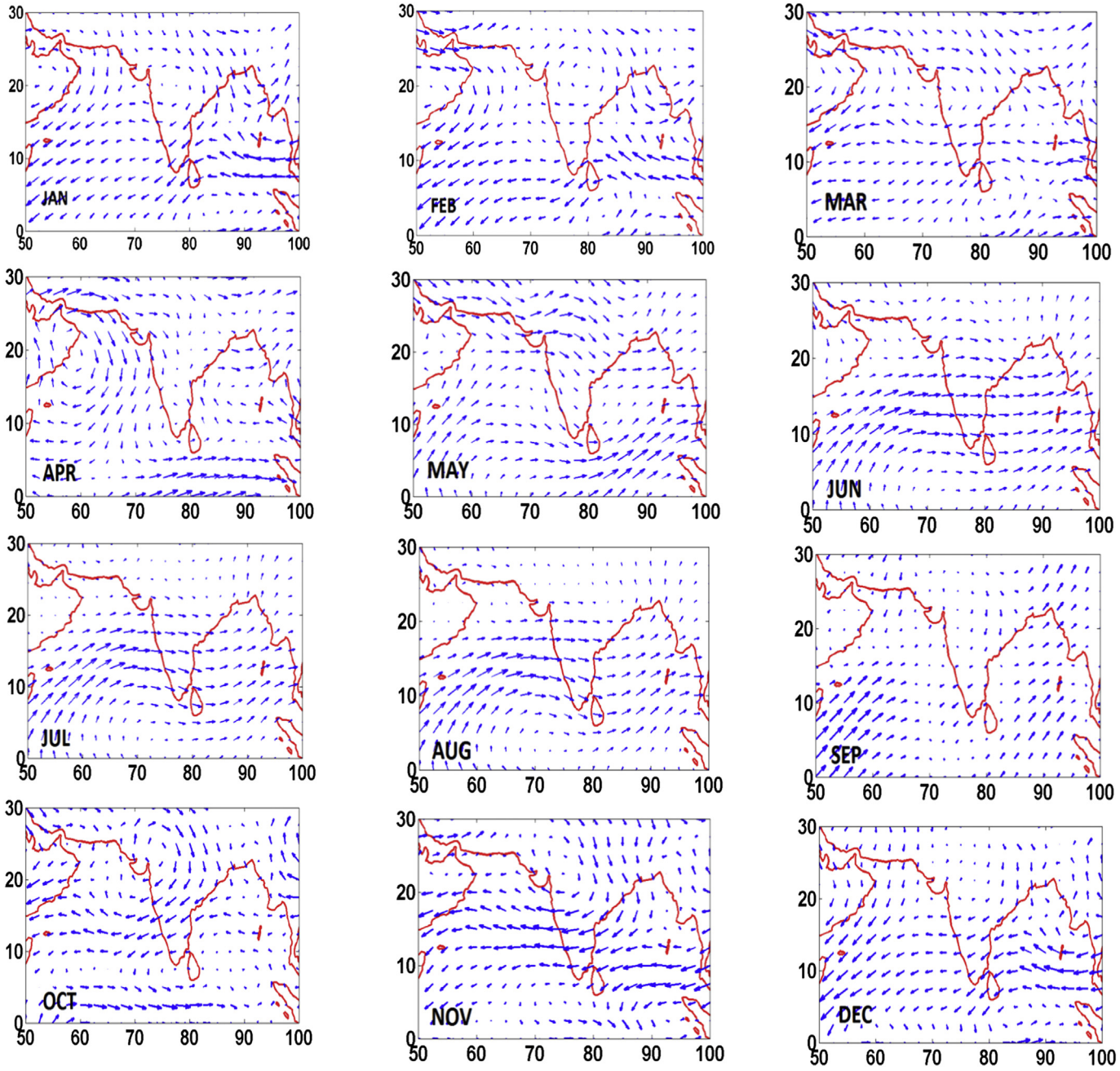

Fig. 11. Mean synoptic wind vectors for different months at 850 mb pressure level over the site during study period.

during the forecast period are mainly due to phenomenon of washout results of lose aerosol particles. The σ_{sp}^{550} value is found to be minimum as 90 M m^{-1} for clear days during the observation period compared to the hazy episodes. This is mainly due to convective causes increasing boundary layer height and dispersion of aerosols. The average σ_{bsp}^{550} is found to be 22 M m^{-1}, 17 M m^{-1} and 5 M m^{-1} for hazy, clear and cloudy periods, respectively. The calculated values show that 14% reduction of σ_{sp}^{550} is during the clear period and 40% reduction during the cloudy period compare to the hazy period. The diurnal variation in $\mathring{A}_{(700/450)}$ at the site has a distinct highest values in the clear days compared to the hazy and cloudy episodes as shown in Fig. 8(c). Fig. 8(c) corresponds to the size of the aerosols and indicate the size of the particles in hazy period are high compare to clear episode and which is due to dust, smoke and vapor. During the cloudy periods, the water vapor content is high in the atmosphere; consequently particles size slightly increases which results in low scattering Ångstrom exponent and indicates the dominance of coarse particles. The $\mathring{A}_{(700/450)}$ average values during the hazy, clear and cloudy periods are 0.79, 1.4 and 0.6 respectively.

5.7. Metrological parameter influence on σ_{sp}^{550}

The scatter plots have been drawn for σ_{sp}^{550} as a function of meteorological parameters like relative humidity (RH), air temperature (AT) and wind speed (WS), respectively, and are shown in Fig. 9(a), (b) and (c). The correlation coefficient $R = 0.53$ has been obtained between σ_{sp}^{550} and RH, which is attributed to hygroscopic

growth of aerosols (Kumar et al., 2010). On other hand AT ($R = -0.56$) and WS ($R = -0.56$) possess negative correlation with σ_{sp}^{550}. High scattering coefficients are therefore likely to occur with certain maximum RH, and at low temperatures. It is found that scattering coefficient observed during the clam wind (wind speed < 0.5 m s^{-1}) condition is remarkably larger than those in strong winds (wind speed > 3 m s^{-1}). For example, average σ_{sp}^{550} in calm wind (0.5 m s^{-1} > wind speed) is double to that of in strong winds. This result highlights that at low wind speeds high aerosol accumulation is observed and strong wind promotes the dilation and dispersion of aerosols.

5.8. Relationship between various aerosol optical properties

In Fig. 10(a), indicates the relation between σ_{sp}^{550} and the respective $Å_{(700/450)}$. The variation of $Å_{(700/450)}$ shows an increase or decrease with aerosol loading at the observational site. Keen analysis of the results reveals that air mass origin and the absence/presence of Indian and Arabian Sea coarse mode intrusion during the monsoon season. High $Å_{(700/450)}$ values measured during the winter season shows the winds contribution for the continental loading from central India. The higher values of $Å_{(700/450)}$ suggest the dominance of fine mode aerosols in the size distribution over the measurement area. The variability in aerosol loading with scattering Ångstrom exponent can be attributed to the changes in aerosol type due to changes in source or changes in contribution of a source (Eck et al., 1999; Dubovik et al., 2002; Toledano et al., 2007). Ramachandran and Rajesh, 2008 reported that the higher values of $Å_{(700/450)}$ over Indian regions, suggest the dominance of fine mode aerosol.

Fig. 10(b), indicates the relation between the backscattering ratio and scattering coefficient. This represents the value of backscattering ratio decreased gradually with increasing scattering coefficient. These observations are in consistent with the findings made by Delene and Ogren (2002) at four different sites in Northern America. The higher values of backscattering ratio at lower aerosol loading indicate the greater contribution from smaller accumulation mode particle (Andrews et al., 2011).

The asymmetry parameter measures the preferred scattering direction (forward or backward) for the light encountering the aerosol particles. The asymmetry parameter approaches $g_\lambda = +1$ for scattering strongly peaked in the forward direction and $g_\lambda = -1$ for scattering strongly peaked in the backward direction. In general, $g_\lambda = 0$ indicates the scattering directions evenly distributed between forward and backward directions. The quantified observations are shown in Fig. 10(c). The scattered plot shows the σ_{sp}^{550} versus asymmetry parameter at 550 nm and is found to have positive correlation ($R = 0.75$). Asymmetry parameter is maximum for large size particles and on the other hand scattering coefficient also increases for large size particles. The high scattering coefficient indicates the increase in the asymmetry parameter. A physical interpretation of Fig. 10(c) highlights that the increase in asymmetry parameter leads to more towards maximum value of 1 (i.e., totally forward scattered light) and reveals the scattering of incoming radiation back is less to its source. This gives an idea that there is a less aerosol forcing effect at the surface.

The aerosol particles have higher median backscattering ratio in the summer suggesting a larger contribution from small accumulation mode aerosol particles and are due to biogenic emission and forest fire influence. The Fig. 10(d) shows negative correlation between asymmetry parameter at 550 nm and backscattering ratio at 550 nm and is found to be $R = -0.96$ over the measurement site. These parameters explain the size distribution of particles over the region. Asymmetry parameter is significantly higher because it is not considered the contribution of the smaller particles (0.1–0.3 μm) which have a larger backscattering component and hence weight the asymmetry parameter toward lower values. When the forward scattering is dominating than the backward scattering, then, asymmetry parameter increases. Larger particles have higher asymmetry parameter. As the larger size particles favors the more forward scattering (i.e. larger g and smaller b) than the smaller one.

Changes in relative humidity affect the real part of the visible-wavelength index of refraction of an aerosol particle and can also affect the particle size distribution by causing particle growth or shrinkage. Thus aerosol backscattering can depend on relative humidity, as well as on aerosol concentration, size distribution spectra and also backscattering at different wavelength. The correlation ($R = 0.87$) between σ_{sp}^{550} and σ_{bsp}^{550} is shown in Fig. 10(e) and exhibits the positive relationship between the parameters. The correlation between σ_{sp}^{550} and black carbon aerosols (BC) concentration has also been studied at observation site and shown in the Fig. 10(f).

The scatter diagram of σ_{sp}^{550} and boundary layer height is shown in Fig. 10(g). The monthly mean Boundary Layer Height (BLH) at 12 UT in a grid of $1.5^\circ \times 1.5^\circ$ is retrieved from the European Centre for Medium – range Weather Forecasts (ECMWF). This gives eight values per day from 0 h to 21 h with an interval of three hours (http//data-portal. ecmwf.int/data/interim daily). The plot shows that boundary layer height was negatively correlated ($R = -0.68$) withσ_{sp}^{550} which plays an important role in building up of aerosols concentration. High scattering coefficient of aerosols is therefore likely to occur with low boundary layer height. The maximum scattering coefficient values are found in winter which signifies the shallow of the boundary layer height.

5.9. Influence of the air mass on the aerosol particles

Airborne particles were detected in the observational site which have been produced locally or transport from somewhere else. In this section, the measured aerosol particles are associated with surface wind paths. The surface wind flow is very important which has influence of the emission sources in the aerosol load type over the site, at the surface aerosol concentration.

Fig. 11 shows the synoptic winds at 850 mb pressure level, covering the entire southern and oceanic regions of India from January to December 2011. It is known that during the winter season, the scattering coefficient values are high, which are due to the winds from west across the central India. Also there is some significant advection from the west coast of India and the Arabian Sea. Consequently the back trajectories transferred the most of the continental particles to the site, thus the fine mode domination occurred during the winter. During winter scattering Ångstrom exponent distribution is also shifted towards larger values >1.0, it indicates the dominance of fine mode aerosol over the sampling site and values lower than <1.0 become much less frequent. The scattering coefficient in the post monsoon is significantly higher than summer due to the increase in the aerosol load which is related to input of fine particle transport from the Indo-Gangetic plain (IGP) to the measurement site (Kumar et al., 2011). During summer most of trajectories are from westerly winds with greater speed (2–4 m s^{-1}) and were found to be dominant which were coming from the Arabian sea. Similar studies have been reported by Reddy et al. (2010).

In the monsoon, minimum scattering coefficient occurs which is due to the southerly winds and are related to oceanic nature transportation from the Arabian oceans. This observation strongly supports the scattering Ångstrom exponent distribution shifts towards the lower values (<1.0) and higher values (>1.0) become much less frequent. These results indicate the long-range transport which play an important role in determining the concentration of aerosols at the observation site.

6. Conclusion

The aerosols light scattering properties near the surface (at about 12 m height), were measured from January to December 2011 at a semi-arid region Anantapur. All parameters investigated in this paper show well defined diurnal, seasonal as well as intra-annual variations. The main conclusions drawn from our study are summarized as follows:

The diurnal average of σ_{sp}^{550} (σ_{bsp}^{550}) was 113 M m^{-1} (14 M m^{-1}) and 104 M m^{-1} (11 M m^{-1}) for weekdays and weekends respectively and found to be 7.8% (11%) reduction in the scattering from weekdays to weekends showing the influence of the submicron aerosols concentration possibly of anthropogenic origin.

The $Å_{(700/450)}$ for weekly was distinctly higher than that of weekend ones. The observed higher values of scattering Ångstrom exponent represent the fine mode domination during the weekdays due to enhancement of anthropogenic activities over the study area.

Spectral dependence of asymmetry parameter was higher at smaller wavelengths and vice versa. High values of asymmetry parameter in the month of October and lower values in March were observed. In the case of backscattering ratio higher values at higher wavelengths and vice versa were noticed. High values of backscattering ratio in the March and low values in October were also observed.

Scattering coefficient is significantly influenced by the meteorological parameters such as WS, AT and RH. A negative correlation has been observed with wind speed and temperature and also positive correlation with relative humidity.

Acknowledgment

The authors wish to thank the Indian Space Research Organization Bangalore, for the financial support is provided by ISRO-GBP under ARFI Project and ISRO-PROWNAM project. R.R. Reddy thanks the University Grants Commission (UGC), New Delhi for granting fellowship under Basic Science Research (BSR) Faculty Scheme during the period of the present study made considerable progress. We would like to acknowledge Dr. K. Krishna Moorthy, Director, Space Physics Laboratory (SPL), Vikram Sarabhai Space Centre (VSSC), Trivandrum for his support and constant encouragement.

References

Anderson, T.L., Ogren, A.J., 1998. Determining aerosol radiative properties using the TSI 3563 integrating nephelometer. Aerosol Sci. Technol. 29, 57–69.

Andreae, M.O., Schmid, O., Yang, H., Chand, D., Yu, J.Z., et al., 2008. Optical properties and chemical composition of the atmospheric aerosol in urban Guangzhou, China. Atmos. Environ. 42, 6335–6350.

Andreae, T.W., Andreae, M.O., Ichoku, C., Maenhaut, W., Cafmeyer, J., Karnieli, A., Orlovsky, L., 2002. Light scattering by dust and anthropogenic aerosol at a remote site in the Negev desert, Israel. J. Geophys. Res. 107 (D2), 4008.

Andrews, E., Ogren, J.A., Bonasoni, P., Marinoni, A., Cuevas, E., Rodríguez, S., Sun, J.Y., Jaffe, D.A., Fischer, E.V., Baltensperger, U., Weingartner, E., Collaud Coen, M., Sharma, S., Macdonald, A.M., Leaitch, W.R., Lin, N.-H., Laj, P., Arsov, T., Kalapov, I., Jefferson, .Sheridan, A.P., 2011. Climatology of aerosol radiative properties in the free troposphere. Atmos. Res. 102, 365–393.

Andrews, E., Sheridan, P.J., Fiebig, M., McComiskey, M., Ogren, J.A., Arnott, P., Covert, D., Ellman, R., Gasparini, R., Collins, D., Jonsson, H., Schmid, B., Wang, J., 2006. Comparison of methods for deriving aerosol asymmetry parameter. J. Geophys. Res. 111. http://dx.doi.org/10.1029/2004JD005734.

Badarinath, K.V.S., Kharol, S.K., Sharma, A.R., 2009. Long-range transport of aerosols from agriculture crop residue burning in Indo-Gangetic Plains – a study using LIDAR, ground measurements and satellite data. J. Atmos. Sol. Terr. Phys. 71, 112–120.

Badrinath, K.V.S., Sharma, A.R., Kaskau tis, D.G., Kharol, S.K., Kambezidis, H.D., 2010. Solar dimming over the tropical urban region of Hyderabad, India: effect of increased cloidiness and increased anthropogenic aerosols. J. Geophys. Res. 115, D21208. http://dx.doi.org/10.1029/2009JD013694.

Balakrishnaiah, G., Raghavendra Kumar, K., Suresh Kumar Reddy, B., Swamulu, C., Rama Gopal, K., Reddy, R.R., Reddy, L.S.S., Nazeer Ahammed, Y., Narasimhulu, K., KrishnaMoorthy, K., Suresh Babu, S., 2011a. Anthropogenic impact on the temporal variations of black carbon and surface aerosol mass concentrations at a tropical semi-arid station in southeastern region of India. J. Asian Earth Sci. 42, 1297–1308.

Balakrishnaiah, G., Raghavendra Kumar, K., Suresh Kumar Reddy, B., Rama Gopal, K., Reddy, R.R., Reddy, L.S.S., Nazeer Ahammed, Y., Narasimhulu, K., KrishnaMoorthy, K., Suresh Babu, S., 2011b. Analysis of optical properties of atmospheric aerosols inferred from spectral AODs and Angstrom wavelength exponent. Atmos. Environ. 45, 1275–1285.

Bergin, M., Cass, G.R., Xu, J., Fang, F., Zeng, L.M., 2001. Aerosol radiative physical, and chemical properties in Beijing during June 1999. J. Geophys. Res. 106, 17969–17980.

Bodhaine, A.B., 1996. Aerosol measurements during the Mauna Loa photochemistry experiment 2. J. Geophys. Res. 101, 14757–14765.

Bodhaine, B.A., Dutton, G.E., 1993. A long-term decrease in Arctic haze at Barrow, Alaska. Geophys. Res. Lett. 20, 947–950.

Boss, E., Pegau, W.S., Lee, M., Twardowski, M.S., Shybanov, E., Korotaev, G., Baratange, F., 2004. The particulate backscattering ratio at LEO-15 and its use to study particle composition and distribution. J. Geophys. Res. 109. C0101410.1029/2002JC001514.

Carrico, C.M., Kus, P., Rood, M.J., Quinn, P.K., Bates, T.S., 2003. Mixtures of pollution, dust, sea salt, and volcanic aerosol during ACE-Asia: radiative properties as a function of relative humidity. J. Geophys. Res. 108, 10.102 9/2003JD003405.

Colland Coen, M., Weingartner, E., Nyeki, S., Cozic, J., Henning, S., Verheggen, B., Gehrig, R., Baltensperger, U., 2007. Long-term trend analysis of aerosol variables at the high-alpine site Jungfraujoch. J. Geophys. Res. 112, D13213. http://dx.doi.org/10.1029/2006JD007995.

Delene, D.J., Ogren, J.A., 2002. Variability of aerosol optical properties at four North American surface monitoring sites. J. Atmos. Sci. 59, 1135–1150.

Dockery, D.W., Pope, C.A., 1996. Epidemiology of acute health effects: summary of time-series. In: Wilson, R., Spengler, J.D. (Eds.), Particles in our air: Concentration and Health Effects. Harvard University Press, Cambridge, MA, USA, pp. 123–147.

Doherty, S.J., Quinn, P.K., Jefferson, A., Carrico, C.M., Anderson, T.L., Hegg, D., 2005. A comparison and summary of aerosol optical properties as ob-served in situ from aircraft, ship, and land during ACE-Asia. J. Geophys. Res. 110, D04201. http://dx.doi.org/10.1029/2004JD004964.

Dubovik, O., Holben, B., Eck, T.F., Smirnov, A., Kaufman, Y.J., King, M.D., Tanré, D., Slutsker, I., 2002. Variability of absorption and optical properties of key aerosol types observed in worldwide locations. J. Atmos. Sci. 59, 590–608.

Eck, T.F., Holben, B.N., Reid, J.S., Dubovik, O., Smirnov, A., O'Neil, N.T., Slutsker, I., Kinne, S., 1999. Wavelength dependence of the optical depth of biomass burning, urban, and desert dust aerosols. J. Geophys. Res. 104 (D24), 31,333–31,349.

Fiebig, M., Ogren, J.A., 2006. Retrieval and climatology of the aerosol asymmetry parameter in the NOAA aerosol monitoring network. J. Geophys. Res. 111, D21204.

Formenti, P., Andreae, M.O., Andreae, T.W., Galani, E., Vasaras, A., Zerefos, C., Amiridis, V., Orlovsky, L., Karnieli, A., Wendisch, M., Wex, H., Holben, B.N., Maenhaut, W., Lelieveld, J., 2001. Aerosol optical properties and large-scale transport of air masses: observations at a coastal and a semiarid site in the eastern Mediterranean during summer 1998. J. Geophys. Res. 106, 9807–9826.

Formenti, P., Andreae, M.O., Lelieveld, J., 2000. Measurements of aerosol optical depth above 3570 m asl in the North Atlantic free troposphere: results from ACE-2. Tellus Ser. B 52, 678–693.

Formenti, P., Boucher, O., Reiner, T., Sprung, F., Andreae, M.O., 2002. STARTE-MED 1998 summer airborne measurements over the Aegean Sea 2. Aerosol scattering and absorption, and radiative calculations. J. Geophys. Res. 107. http://dx.doi.org/10.1029/2001J D 001536.

Foster, P., Ramaswamy, V., Artaxo, P., Berntsen, T., Betts, R., Fahey, D.W., Haywood, J., Lean, J., Lowe, D.C., Myhre, G., Nganga, J., Prinn, R., Raga, G., Schulz, M., Van Dorland, R., 2007. Changes in atmospheric constituents and in radiative forcing. In: Solomon, S., Qin, D., Manning, M., Chen, Z., Marquis, M., Averyt, K.B., Tignor, M., Miller, H.L. (Eds.), Climate Change 2007: the Physical Science Basis, Contribution of Working Group I to the Fourth Assessment Report of the Intergovernmental Panel on Climate Change. Cambridge University Press, Cambridge, United Kingdom and New York, NY, USA.

Haywood, J., Shine, K.P., 1997. Multi-spectral calculations of the direct radiative forcing of tropospheric sulphate and soot aerosols using a column model. Quarterly J. R. Meteorol. Soc. 123, 1907–1930.

Haywood, J.M., Ramaswamy, V., 1998. Global sensitivity studies of the direct radiative forcing due to anthropogenic sulfate and black carbon aerosols. J. Geophys. Res. 103 (D6), 6043–6058.

Horvath, H., 1995. Estimation of the average visibility in central Europe. Atmos. Environ. 29, 241–246.

Intergovernmental Panel on Climate Change (IPCC), 2007. Climate change 2007: the physical science basis. In: Solomon, S., et al. (Eds.), Contribution of Working Group I to the Fourth Assessment Report of the Intergovernmental Panel on Climate Change. Cambridge Univ. Press, Cambridge and New York, p. 996.

Jung, J., Lee, H., Kim, Y.J., Liu Zhang, X., 2009. Optical properties of atmospheric aerosols obtained by in situ and remote measurements during 2006 Campaign of Air Quality Research in Beijing (CAREBeijing-2006). J. Geophys. Res. 114, 10. 1029/2008JD010337.

Kaufman, Y.J., Koren, I., Remer, L.A., Rosenfeld, D., Rudich, Y., 2005. The effect of smoke, dust, and pollution aerosol on shallow cloud development over the Atlantic Ocean. Proc. Natl. Acad. Sci. U. S. A. 102 (32), 11207–11212.

Kumar, K.R., Narasimhulu, K., Balakrishnaiah, G., Suresh Kumar Reddy, B., Rama Gopal, K., Reddy, R.R., Satheesh, S.K., KrishnaMoorthy, K., Suresh Babu, S., 2010. A study on the variations of optical and physical properties of aerosols over tropical semi-arid station during grassland fire. Atmos. Res. 95, 77–87.

Kumar, K.R., Narasimhulu, K., Balakrishnaiah, G., Suresh Kumar Reddy, B., Rama Gopal, K., Reddy, R.R., Satheesh, S.K., KrishnaMoorthy, K., Suresh Babu, S., 2011. Characterization of aerosol black carbon over a tropical semi-arid region of Anantapur, India. Atmos. Res. 100, 12–27.

Latha, K.M., Badarinath, K.V.S., 2005. Seasonal variations of black carbon aerosols and total aerosol mass concentrations over urban environment in India. Atmos. Environ. 39, 4129–4141.

Lyamani, Omlmoa, F.J.H., Alados-Arboledas, L., 2008. Light scattering and absorption properties of aerosol particles in the urban environment of Granada, Spain. Atmos. Environ. 42, 2630–2642.

Pandithurai, G., Dipu, S., Dani, K.K., Tiwari, S., Bisht, D.S., Devara, P.C.S., Pinker, R.T., 2008. Aerosol radiative forcing during dust events over New Delhi, India. J. Geophys. Res. 113, D13209,. http://dx.doi.org/10.1029/2008JD009804.

Parameswaran, K., Rajan, Rekha, Vijayakumar, G., Rajeev, K., Krishna Moorthy, K., Nair, Prabha R., Satheesh, S.K., 1998. Seasonal and long term variations of aerosol content in the atmospheric mixing region at a tropical station on the Arabian sea-coast. J. Atmos. Sol. Terr. Phys. 60, 17–25.

Pathak, B., Kalita, G., Bhuyan, K., Bhuyan, P.K., Moorthy, K.K., 2010. Aerosol temporal characteristics and its impact on shortwave radiative forcing at a location in the northeast of India. J. Geophys. Res. 115, D19204. http://dx.doi.org/10.1029/2009JD013462.

Pereira, S.N., Wagner, F., Silva, A.M., 2011. Seven years of measurements of aerosol scattering properties, near the surface, in the southwestern Iberia Peninsula. Atmos. Chem. Phys. 11, 17–29.

Ramachandran, S., Rajesh, T.A., 2008. Asymmetry parameters in the lower troposphere derived from aircraft measurements of aerosol scattering coefficients over tropical India. J. Geophys. Res. 113. http://dx.doi.org/10.1029/2008JD009795.

Reddy, B.S.K., Raghavendra Kumar, K., Balakrishnaiah, G., Rama Gopal, K., Reddy, R.R., Nazeer Ahammed, Y., Narasimhulu, K., Siva Sankara Reddy, L., Lal, Shyam, 2010. Observational studies on the variations in surface ozone concentration at Anantapur in southern India. Atmos. Res. 98, 125–139.

Schwartz, S.E., Arnold, F., Blanchet, J.P., Durke, P.A., Hormann, D.J., Hoppel, W.A., King, M.D., Lacis, A.A., Nakajima, T., Ogren, J.A., Toon, O.B., Wendisch, M., 1995. Group report: concentration between aerosol properties and forcing of climate. In: Heintzenderg, J., Charlson, R.J. (Eds.), Aerosol of Climate. Wiley, New York, pp. 251–280.

Toledano, C., Cachorro, V.E., Berjon, A., de Frutos, A.M., Sorribas, M., de la Morenab, B.A., Goloub, P., 2007. Aerosol optical depth and Ångström exponent climatology at El Arenosillo AERONET site (Huelva, Spain). Quarterly J. R. Meteorol. Soc. 133, 795–807.

Twardowski, M.S., Boss, E., Macdonald, J.B., Pegau, W.S., Barnard, A.H., Zaneveld, J.R.V., 2001. A model for estimating bulk refractive index from the optical backscattering ratio and the implications for understanding particle composition in case I and case II waters. J. Geophys. Res. 106, 14,129–14,142.

Wiscombe, W.J., Grams, G., 1976. The backscattered fraction in two-stream approximations. J. Atmos. Sci. 33, 2440–2451.

Xu, J., Bergin, M.H., Yu, X., Liu, G., Zhao, J., Carrico, C.M., Bauman, K., 2002. Measurement of aerosol chemical, physical and radiative properties in the Yangtze delta region of China. Atmos. Environ. 36, 161–173.